Supporting Information

Dioxygen Activation at Non-Heme Diiron Centers: Oxidation of a Proximal Residue in the I100W Mutant of Toluene/*o*-Xylene Monooxygenase Hydroxylase

Leslie J. Murray,[1] Ricardo García-Serres,[2] Michael S. McCormick,[1] Roman Davydov,[3] Sunil Naik,[2] Sun-Hee Kim,[3] Brian M. Hoffman,[3] Boi Hanh Huynh,[2] and Stephen J. Lippard[1]

[1]Department of Chemistry, Massachusetts Institute of Technology, Cambridge, MA, [2]Department of Physics, Emory University, Atlanta, GA, and [3]Department of Chemistry, Northwestern University, Evanston, IL

lippard@mit.edu; vhuynh@physics.emory.edu; and bmh@northwestern.edu

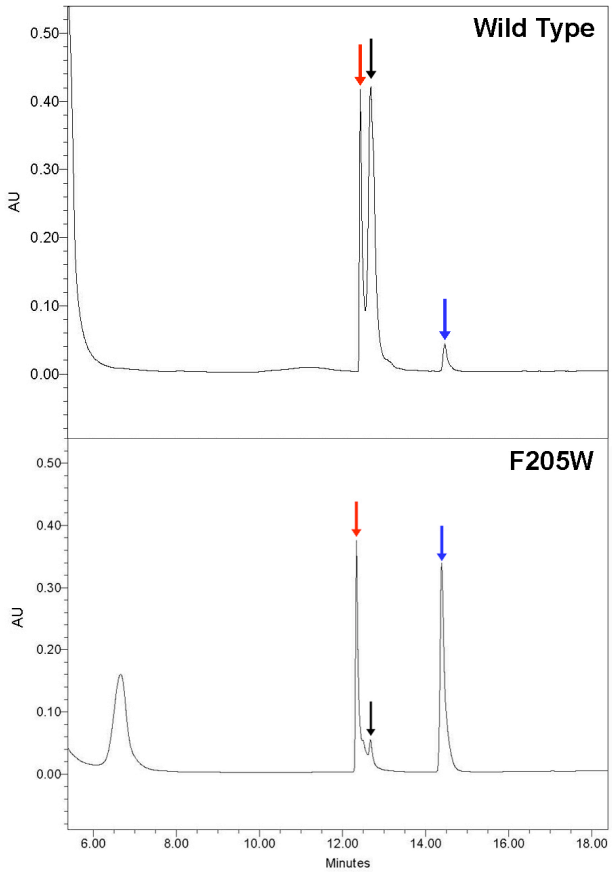

Figure S1. HPLC traces at 280 nm of steady-state reaction mixtures for wild-type and F205W mutant hydroxylases. Catechol (black arrow) is the only observed product in reactions. The peak corresponding to phenol (blue arrow), the substrate used in these assays, was of a lower intensity in the reaction containing the F205W mutant, consistent with the reduced steady-state activity of this hydroxylase. The compound eluting at 6 min does not arise from hydroquinone, as determined by HPLC traces for samples doped with this compound. A background peak at ~ 12.5 min (red arrow) appears in all traces with equal intensity.

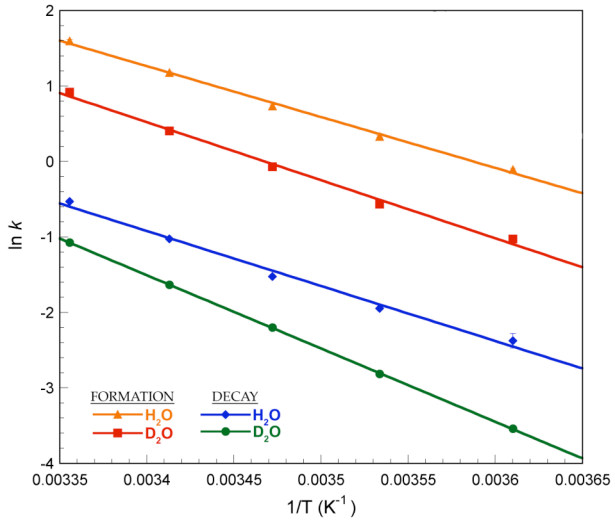

Figure S2. Arrhenius plots for formation and decay rates of the mixed-valent diiron(III,IV)–W$^{\bullet}$ formed during the reaction of $ToMOH_{red}$ I100W:3ToMOD with dioxygen. The difference in activation energy for both phases in protic versus deuterated buffers is non-zero as determined from the Arrhenius plots (right). The temperature dependence of k_H/k_D is therefore non-zero for both processes with the decay exhibiting a stronger dependence than formation. This data imply that hydrogen atom transfer or tunneling from W100 to the diiron(III) intermediate does not occur during formation.

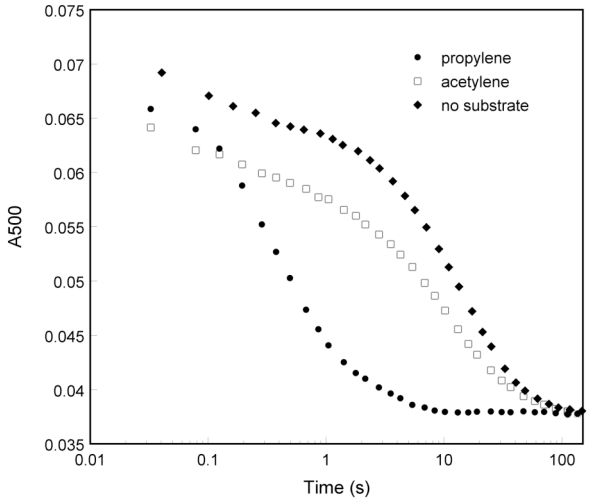

Figure S3. Effect of propylene and acetylene on the decay rate of the tryptophanyl radical. Propylene, a substrate for $MMOH_{peroxo}$, accelerates k_d by more than 50-fold to 2.8 s^{-1} whereas acetylene has only a minor effect.

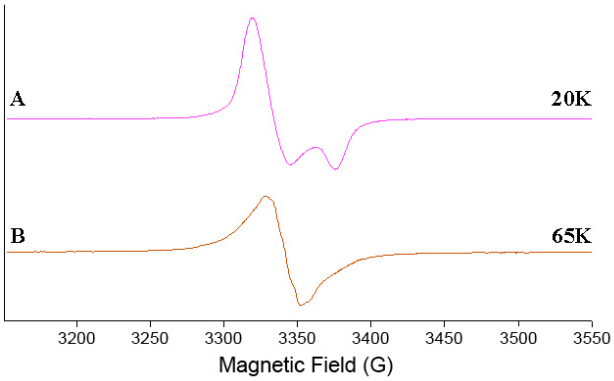

Figure S4. X-band EPR spectra of the diiron(III,IV)–W$^{\bullet}$ species at (**A**) 20 K and (**B**) 65 K. (**A**) The spectrum at 20 K contains the anisotropic features associated with the diiron center with the radical signal saturated. (**B**) The spectrum at 65 K of the intermediate predominantly arises from the W$^{\bullet}$ radical. The diiron center is not saturated below 60 K.

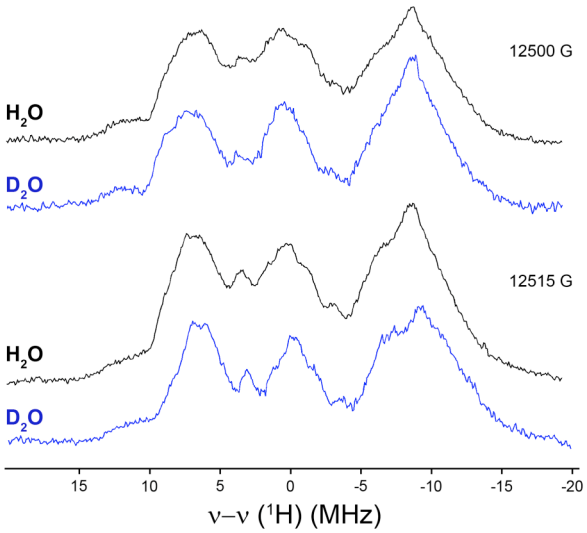

Figure S5. ^{1}H-Mims ENDOR spectra of the tryptophan radical in buffers containing H_2O (black) and D_2O (blue). The two spectra are superimposable indicating that there are no exchangeable protons on the radical. The spectra, as for the ^{2}H-Mims spectra, are dominated by signals from the indole protons.

Ion	Mass (m/z)	Charge
b4	341.2	+1
b5	527.2	+1
b6	626.3	+1
b6	313.2	+2
b7	713.3	+1
b20	*1122.5*	*+2*
b22	*1239.6*	*+2*

Ion	Mass (m/z)	Charge
y1	175.1	+1
y2	246.2	+1
y3	375.2	+1
y4	446.3	+1
y5	547.3	+1
y6	634.3	+1
y7	705.4	+1
y8	776.4	+1
y9	939.5	+1
y12	1320.6	+1
y19	*1055.8*	*+2*
y23	*1278.6*	*+2*
y27	*1328.2*	*+2*
y27	*999.1*	*+3*

Figure S6. ESI-MS/MS fragment ions arising from the tryptic peptide containing W100. The fragment peptide ions of the tryptic peptide of interest are labeled using the b and y ion nomenclature (top). W100 is in red font. The $[M+H]^{3+}$ parent ion was fragmented. The fragment peptide ions were assigned based on mass and isotopic spacing of the individual envelopes. The fragment ions containing the modified residue are shown in italics. This analysis revealed that the 16 Da increase observed for the reacted sample results from modification of a residue situated between H96 and E104.

Table S1. Sequences for Mutagenic Primers for the α-Subunit of ToMOH

MUTATION	PRIMER	SEQUENCE (5' to 3')
I100W	sense	caacttcacttcggagcg**TGG**gcacttgaagaatacg
	antisense	cgtattcttcaagtgc**CCA**cgctccgaagtgaagttg
I100Y	sense	ggttagcactatgcaacttcacttcggagcg**TAT**gcacttgaagaatacg
	antisense	cgtattcttcaagtgc**ATA**cgctccgaagtgaagttgcatagtgctaacc
F205W	sense	ggcttcaccaatatgcag**TGG**ctcggtttggccg
	antisense	cggccaaaccgag**CCA**ctgcatattggtgaagcc
L208F	sense	gcagtttctcggt**TTC**cgccgctgacgctgctgaggccg
	antisense	cggcctcagcagcgtcagcggc**GAA**accgagaaactgc

Table S2. Data Collection and Refinement Statistics for ToMOH I100W

	$ToMOH_{ox}$
Data Collection	
Beamline	SSRL 9-2
Wavelength (Å)	0.979
Space Group	$P3_121$
Unit cell dimensions (Å)	182.4 x 182.4 x 68.0
Resolution range (Å)	50 - 2.1
Total Reflections	449931
Unique Reflections	70195
Completeness (%)*	84.7 (83.6)
I/s(I)	27.2 (19.4)
Rsym (%)	6.4 (54.1)
Phasing method	Molecular Replacement
Refinement	
Rcryst (%)	21.7
Rfree (%)	28.4
No. Protein Atoms	7352
No. Non-Protien Atoms	204
r.m.s deviation bond length (Å)	0.034
r.m.s deviation bond angles (°)	2.76
Average B-value ($Å^2$)	50.8

Table S3. Distances Between the Atoms of the Side-Chain of W100 and the Diiron Active Site

Position A Distances (Å)	C_α	C_β	C_γ	$C_{\delta1}$	$C_{\delta2}$	$C_{\varepsilon2}$	$C_{\varepsilon3}$	$C_{\zeta2}$	$C_{\zeta3}$	$C_{\eta2}$	N_ε
Fe1	8.8	8.1	9.0	9.7	9.3	10.3	9.2	11.1	10.1	11.0	10.5
Fe2	10.6	10.0	10.6	11.4	10.6	11.5	10.1	11.9	10.7	11.6	11.9
μ-OH (hydroxide)	10.3	9.5	10.1	10.8	10.4	11.2	10.2	11.8	10.9	11.7	11.4
μ-OH (glycerol)	8.5	7.8	8.5	9.4	8.6	9.6	8.2	10.2	8.9	9.9	10.0
H_2O (terminal on Fe1)	8.3	7.3	7.9	8.5	8.2	9.0	8.3	9.8	9.1	9.8	9.1
Position B Distances (Å)	C_α	C_β	C_γ	$C_{\delta1}$	$C_{\delta2}$	$C_{\varepsilon2}$	$C_{\varepsilon3}$	$C_{\zeta2}$	$C_{\zeta3}$	$C_{\eta2}$	N_ε
Fe1	8.7	8.2	8.0	8.9	7.2	7.7	6.3	7.5	6.0	6.7	8.7
Fe2	10.6	10.2	9.7	10.4	8.5	8.7	7.6	8.0	6.8	7.0	9.7
μ-OH (hydroxide)	10.3	9.6	9.2	9.9	8.3	8.5	7.5	8.1	7.0	7.3	9.5
μ-OH (glycerol)	8.4	8.1	7.6	8.4	6.5	6.9	5.5	6.3	4.9	5.3	8.0
H_2O (terminal on Fe1)	8.2	7.4	6.9	7.6	6.2	6.5	5.7	6.3	5.5	5.8	7.3

Table S4. Formation and Decay Rate Constants for I100W Transient in H_2O and D_2O Buffers

Temp (± 0.1 °C)	H_2O		D_2O		Formation	Decay
	k_f (s^{-1})	k_d (s^{-1})	k_f (s^{-1})	k_d (s^{-1})	k_H / k_D	k_H / k_D
4.0	0.90 ± 0.01	0.093 ± 0.009	0.358 ± 0.002	0.029 ± 0.001	2.51 ± 0.04	3.2 ± 0.3
10.0	1.39 ± 0.02	0.143 ± 0.002	0.567 ± 0.003	0.060 ± 0.001	2.46 ± 0.03	2.36 ± 0.05
15.0	2.09 ± 0.03	0.218 ± 0.002	0.93 ± 0.04	0.111 ± 0.001	2.24 ± 0.08	1.97 ± 0.02
20.0	3.25 ± 0.05	0.359 ± 0.008	1.50 ± 0.06	0.195 ± 0.001	2.17 ± 0.09	1.84 ± 0.04
25.0	4.9 ± 0.1	0.59 ± 0.01	2.50 ± 0.07	0.342 ± 0.001	1.97 ± 0.07	1.72 ± 0.02

Table S5. Formation and Decay Rate Constants at Varying pH Values

pH	k_f (s^{-1})	k_d (s^{-1})
6.5	0.66 ± 0.01	0.0417 ± 0.0006
6.6	0.71 ± 0.01	0.052 ± 0.005
7.0	0.86 ± 0.04	0.070 ± 0.003
7.2	1.05 ± 0.02	0.095 ± 0.001
7.5	1.13 ± 0.02	0.091 ± 0.001